A thermionic-emission-diffusion model for graded base *Pnp* heterojunction bipolar transistors

S. Datta, K. P. Roenker,[a] and M. M. Cahay
Department of Electrical and Computer Engineering, University of Cincinnati, Cincinnati, Ohio 45221-0030

(Received 2 December 1997; accepted for publication 10 March 1998)

An analytical model which matches thermionic-emission-diffusion of holes across the emitter-base heterojunction with drift-diffusion transport across a graded base has been developed and used to examine the performance capabilities of InP-based *Pnp* heterojunction bipolar transistors (HBTs). Hole drift-diffusion across the emitter-base space charge region is shown to be of comparable importance to thermionic emission in controlling hole injection into the base. The effects of compositional base grading on the recombination currents is also taken into account. Compositional grading of the base is shown to enhance the device's current gain by as much as a factor of 10 by reducing recombination in the quasi-neutral base. More importantly, compositional base grading significantly reduces the base transit time which improves the device's peak cutoff frequency by as much as a factor of 1.5. A cutoff frequency as high as 35 GHz is found to be possible. The analysis indicates that composition grading of the base can be useful in developing high performance *Pnp* InP-based HBTs. © *1998 American Institute of Physics.* [S0021-8979(98)01112-8]

I. INTRODUCTION

In comparison with *Npn* heterojunction bipolar transistors (HBTs), *Pnp* InP-based HBTs have not been extensively investigated. However, the *Pnp* devices are of interest for some circuit applications where they can be monolithically integrated with *Npn* HBTs and used as active loads or in push-pull amplifiers.[1–3] They have also shown promise for power amplifiers.[4–7] Recently, there have been several reports of successful demonstrations of InP-based *Pnp* HBTs operating at microwave frequencies.[8–10] Stanchina *et al.*[8,9] have reported InAlAs/InGaAs *Pnp* HBTs with a current gain as high as 170, a cutoff frequency f_T of 14 GHz, and a maximum frequency of oscillation f_{MAX} of 22 GHz. Lunardi *et al.*[10] have reported similar results for InP/InGaAs *Pnp* HBTs with a current gain as high as 420, a cutoff frequency f_T of 10.5 GHz, and a maximum frequency of oscillation f_{MAX} of 25 GHz. In addition, the monolithic integration of *Pnp* HBTs with *Npn*'s has also been recently demonstrated using a selective area epitaxial growth.[8] There have also been some theoretical studies of the devices using numerical modeling to investigate the device's performance potential.[11,12] Finally, some encouraging results have also been reported for *Pnp* HBTs in the similar AlGaAs/GaAs material system in recent years.[13,14]

This article investigates the performance of the *Pnp* InP-based HBTs by developing an analytical thermionic-emission-diffusion model which matches the hole drift-diffusion current at the emitter end of the quasi-neutral, compositionally graded base with the hole thermionic-emission-diffusion current across the valence band spike. The result is then used to determine the excess hole concentration at the emitter end of the base. This approach is easily extended to GaAs-based *Pnp* HBTs and is analogous to that previously employed for the *Npn* HBT.[15–17] In addition, the model incorporates the effects of compositional grading in the base which is needed to enhance hole transport for high speed devices.[18–20] In Sec. II we describe the development of the thermionic-emission-diffusion model and derive expressions for the hole profile and the hole drift-diffusion current in the base. In Sec. III the terminal currents are developed including the effects of compositional grading on the base recombination currents, and the current gain is calculated. The effect of compositional grading on the base transit time is calculated in Sec. IV along with the other transit time components to determine the emitter-to-collector delay time and the cutoff frequency. Section V presents numerical results for an InAlAs/InGaAs *Pnp* HBT similar to that reported by Stanchina *et al.*,[8,9] but incorporating compositional grading in the base. In Sec. VI we draw conclusions and discuss the performance limitations and prospects for the *Pnp* HBTs as indicated by the model.

II. THERMIONIC-EMISSION-DIFFUSION MODEL

This development of an analytical model for the *Pnp* HBT follows that previously reported for the *Npn* HBT[16–19] and earlier studies of the *Pnp* HBT.[6,7,21–23] In particular, this approach follows that of Grinberg *et al.*[16,17] where the electron thermionic-field-emission current across the heterojunction spike at the emitter-base heterojunction is matched with the diffusion current in the base to derive the excess carrier concentration at the emitter end of the quasi-neutral base. In this article an analogous approach is followed for the holes based on a more general description of carrier injection across the heterojunction following Stettler and Lundstrom.[15] In particular, the drift diffusion of holes across the emitter space charge region is included and found to be as important as thermionic emission in limiting hole injection into the base. Subsequently, the drift-diffusion model is employed to

[a]Electronic mail: kroenker@ece.uc.edu

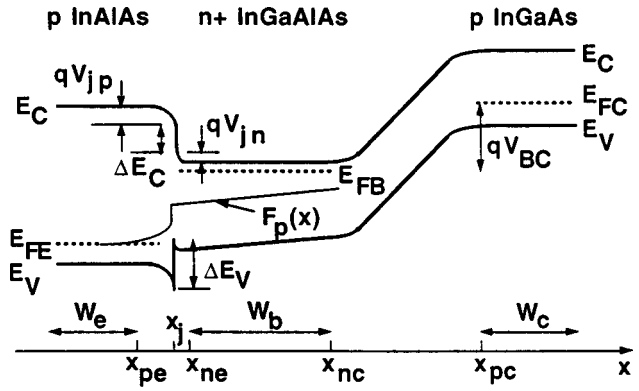

FIG. 1. Schematic energy band diagram and coordinate system for *Pnp* heterojunction bipolar transistor in a forward active mode. Also shown is the spatial dependence of the hole quasi-Fermi level $F_p(x)$ across the device.

describe hole transport across the quasi-neutral base where the effects of compositional grading have been included. This article extends the work of Hutchby,[21] Sunderland and Dapkus,[22] and Yuan[23] by including: (1) the physics of hole thermionic-emission-diffusion injection at the emitter-base heterojunction, (2) the effects of linear compositional grading in the base, and (3) the calculation of the recombination currents in the base current including the effects of compositional grading. In addition, it incorporates a more realistic boundary condition for the hole concentration at the collector end of the quasi-neutral base, i.e., a finite concentration sufficient to carry the hole collector current.[24] As a result, this model provides a more comprehensive and accurate description of the operation of the *Pnp* HBT for use in device design and for comparison with experimental results.

In this model we assume an abrupt emitter-base heterojunction, with a linearly graded base region to enhance hole transport. Shown in Fig. 1 is the energy band diagram and coordinate system employed in this analysis. Also shown is the hole quasi-Fermi level. Following Ryum and Abdel-Motaleb's analysis for an *Npn* with a compositionally graded base,[18] we can write for the hole and electron current densities

$$J_p = -\mu_p p(x)\frac{d}{dx}[qV(x)+\chi(x)+E_g(x)] - qD_p\frac{dp(x)}{dx}, \tag{1}$$

$$J_n = -\mu_n n(x)\frac{d}{dx}[qV(x)+\chi(x)] + qD_n\frac{dn(x)}{dx}, \tag{2}$$

where $V(x)$ is the electrostatic potential, q is the magnitude of the electronic charge, $\chi(x)$ is the electron affinity, $E_g(x)$ is the energy band gap, μ_p (μ_n) is the hole (electron) mobility, D_p (D_n) is the hole (electron) diffusion constant, and $p(x)$ and $n(x)$ are the hole and electron carrier concentrations, respectively. Within the heavily doped n^+ base, the majority carrier electron current can be approximated as being negligibly small ($J_n=0$) so that from Eq. (2) we can write using Einstein's relation

$$\frac{k_BT}{n(x)}\frac{dn(x)}{dx} = \frac{d}{dx}[qV(x)+\chi(x)]. \tag{3}$$

In the quasi-neutral base, we have charge neutrality satisfied so that

$$p(x)+N_B(x)=n(x). \tag{4}$$

For a uniformly doped base, the electron and hole density gradients are equal from Eq. (4) and we can rewrite Eq. (3) using Eq. (4) as

$$\frac{k_BT}{p(x)+N_B}\frac{dp(x)}{dx} = \frac{d}{dx}[qV(x)+\chi(x)]. \tag{5}$$

Substituting Eq. (5) into Eq. (1) we can obtain the following expression for the hole current density:

$$J_p = -qD_p\left[\frac{2p(x)+N_B}{p(x)+N_B}\right]\frac{dp(x)}{dx} + \frac{qD_p}{L_g}p(x), \tag{6}$$

where, assuming a linearly graded base region, we can define a base grading length L_g given by

$$\frac{1}{L_g} \equiv \frac{E_g(x_{ne})-E_g(x_{nc})}{k_BTW_b}, \tag{7}$$

where W_b is the width of the quasi-neutral base, and $E_g(x_{ne})$ and $E_g(x_{nc})$ are the base energy band gaps at the emitter and collector ends, respectively. For low level hole injection into the base, i.e., $p(x) \ll N_B$, we can neglect the hole contribution in the prefactor in the first term in Eq. (6). Rearranging Eq. (6) and integrating across the width of the quasi-neutral base, we can then express the hole current density in terms of the hole concentrations at the opposite ends of the base and the grading length as given below

$$J_p = \frac{qD_p}{L_g(e^{W_b/L_g}-1)}[p(x_{ne})e^{W_b/L_g} - p(x_{nc})]. \tag{8}$$

We can now substitute Eq. (8) back into Eq. (6) and integrate to determine the hole concentration profile in the base from which we obtain

$$p(x) = p(x_{ne})\left[\frac{e^{W_b/L_g}-e^{(x-x_{ne})/L_g}}{e^{W_b/L_g}-1}\right] + p(x_{nc}) \times\left[\frac{e^{(x-x_{ne})/L_g}-1}{e^{W_b/L_g}-1}\right]. \tag{9}$$

The hole concentrations at the ends of the base must now be related to the junction biases in order to make Eq. (9) useful. To accurately describe the hole injection across the emitter-base heterojunction, the thermionic-emission-diffusion theory is used following Stettler and Lundstrom.[15] The hole thermionic-emission-diffusion current is then given by[15]

$$J_p = \frac{qp_0(\chi_{ne})}{\left\{\frac{1}{S_{ip}}+\frac{1}{S_{ep}}+\frac{1}{S_{dp}}+\frac{1}{v_s}\right\}}e^{qV_{EB}/k_BT}, \tag{10}$$

where $p_0(x_{ne})$ is the thermal equilibrium hole concentration at the emitter end of the quasi-neutral base, v_s corresponds to the saturation velocity of holes in the base-collector space charge region assuming the device is biased in the forward active mode and the S's are the effective hole velocities described below. The result given by Eq. (10) is analogous to

that derived for electron injection across an $N-p$ heterojunction by Stettler and Lundstrom.[15] For the electron injection case, the thermionic emission velocity S_{in} is normally the smallest and so controls the electron current density injected into the base.[15–19] However, for the case of hole injection in Pnp HBTs considered here, the situation is not as clear. We first define the effective hole velocities below and then compare their magnitudes.

Thermionic-field-emission of holes across the valence band spike, including tunneling effects, gives rise to the effective hole interface velocity S_{ip} given by

$$S_{ip}=\gamma_h v_h e^{-(\Delta E_V - qV_{jn})/k_BT}, \tag{11}$$

where γ_h is the hole tunneling factor calculated following Grinberg *et al.*,[16] ΔE_v is the valence band discontinuity, V_{jn} gives the band bending on the base side of the emitter-base heterojunction and v_h is the mean thermal hole velocity given by $v_h \equiv \sqrt{(k_BT)/(2\pi m_h^*)}$, where m_n^* is the hole density of states effective mass in the base. In deriving Eq. (11), since the hole effective mass is very nearly the same in the emitter and the base for the InP-based materials, the valence band densities of states in the emitter and base are nearly equal and their difference has been neglected.

The second effective velocity in Eq. (10) is the hole drift-diffusion velocity in the emitter space charge region S_{ep} given by

$$S_{ep}=\mu_h E(x_j^-) e^{-(\Delta E_V - qV_{jn})/k_BT}, \tag{12}$$

where μ_h is the low field hole mobility in the emitter and $E(x_j^-)$ is the magnitude of the electric field on the emitter side of the heterojunction interface. The third velocity S_{dp} corresponds to the effective hole velocity associated with drift diffusion across the quasi-neutral base region, which is dependent on the extent of base grading and is given by

$$S_{dp}=\frac{v_s e^{W_b/L_g}}{[1+v_s L_g/D_p(e^{W_b/L_g}-1)]}. \tag{13}$$

From (10) it is apparent that the smallest of the effective hole velocities determines the hole thermionic-emission-diffusion current J_p. To illustrate this, shown in Fig. 2 is a plot of the four-hole velocities as a function of the emitter-base bias for the device structure of Stanchina *et al.*[8] where there is no compositional grading in the base. In Fig. 2 the hole saturation velocity v_s (4.5×10^6 cm/s) assumed is somewhat smaller than that for electrons (10^7 cm s),[12] but much larger than the other velocities and so is less important in determining the hole injection current. Similarly, for the case considered here (no compositional grading), the hole diffusion velocity S_{dp} is larger than either S_{ip} or S_{ep} so that hole diffusion across the base is limited by the extent of hole injection across the emitter-base junction. As a result, the remaining two-hole velocities S_{ip} or S_{ep} in Eq. (10) largely determine the hole current density. Shown in Fig. 2 is the thermionic-emission velocity S_{ip} with and without inclusion of the hole tunneling factor γ_h. The effect of hole tunneling is to enable additional hole injection across the heterojunction so that it effectively raises the velocity S_{ip}. The effect is significant; tunneling increases S_{ip} by more than a factor 10 at low bias, but decreases to approximately a factor of 2 at high bias. For holes, the low field mobility is much smaller than that for electrons so the velocity prefactor in Eq. (12) makes S_{ep} smaller and comparable to the thermionic-emission velocity S_{ip} including tunneling as seen in Fig. 2. As a result, the drift diffusion of holes across the emitter space charge region is comparable in importance to thermionic emission across the valence band discontinuity in limiting the hole injection into the base. This is in contrast to the case for electron injection into the base in Npn HBTs where the velocity S_{in} is the smallest and thermionic emission across the conduction band discontinuity is the dominant limiting process.[16]

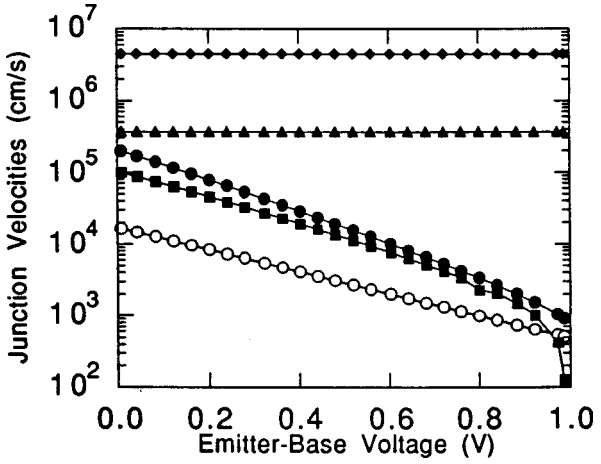

FIG. 2. Effective hole velocities [emitter space charge region drift diffusion (■), thermionic emission without (○) and with (●) tunneling, quasi-neutral base diffusion (▲) and base-collector saturation velocity (♦)] for InAlAs/InGaAs Pnp HBT as a function of emitter-base bias V_{EB} for the case of no compositional base grading.

Shown in Fig. 3 is the effect of compositional grading on the effective hole velocities calculated at a fixed collector current density of 10^4 A/cm^2. For the effective hole velocity S_{dp} describing drift diffusion across the neutral base defined in Eq. (13), the velocity rises and then saturates since the quasi-electric field generated by the compositional grading

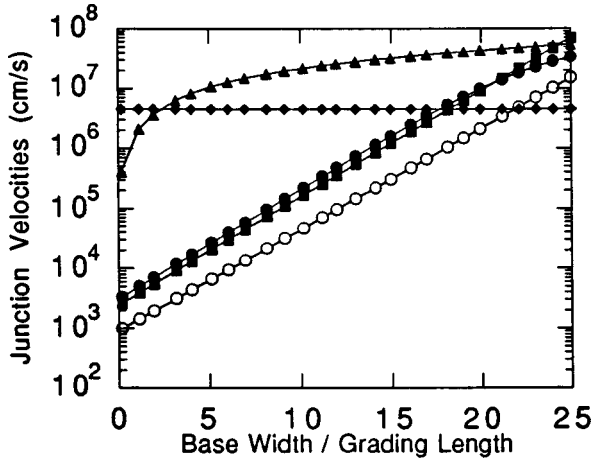

FIG. 3. Effective hole velocities [emitter space charge region drift diffusion (■), thermionic emission without (○) and with (●) tunneling, quasi-neutral base diffusion (▲) and base-collector saturation velocity (♦)] in InAlAs/InGaAs Pnp as a function of compositional grading (W_b/L_g) in the base.

aids the hole transport across the base. The hole velocities S_{ip} and S_{ep} are also a function of the compositional grading in the base and show a steady increase with larger grading. The origin of this effect can be understood as follows. Since the emitter energy band gap is fixed (1.47 eV for lattice matched InAlAs), as the extent of compositional grading in the base increases, the valence band discontinuity decreases and the emitter-base junction built-in potential increases so that the thermionic emission velocity S_{ip} given by Eq. (11) and the emitter drift-diffusion velocity S_{ep} given by Eq. (12) increase. However, they both remain less than S_{dp} and so their processes continue to control the hole current flow across the emitter-base heterojunction until the base grading becomes large ($W_b/L_g>15$).

Before matching the hole drift-diffusion current in the base given by Eq. (8) with the thermionic-emission-diffusion current given by Eq. (10) to determine the hole concentration at the emitter end of the quasi-neutral base, we follow Das[24] and impose the constraint that the hole concentration at the collector end of the base be at least sufficient to carry the hole current, i.e.,

$$p(x_{nc})=\frac{J_p}{qv_s}, \tag{14}$$

where v_s is the hole saturation velocity in the base-collector space charge region. Neglected in Eq. (14) is the effect of the base-collector bias V_{CB} so that Eq. (14) is not accurate for the device operating in the forward saturation mode. Substituting Eq. (14) into Eq. (8) and rearranging we get a modified result for the hole drift-diffusion current in the base which is only a function of the hole concentration at the emitter end of the base and the device structure parameters and is given by

$$J_p=\frac{qv_s e^{W_b/L_g}}{1+(v_sL_g/D_p)(e^{W_b/L_g}-1)}\,p(x_{ne})=qS_{dp}p(x_{ne}). \tag{15}$$

Equation (15) is the origin of the definition of the effective hole velocity S_{dp} associated with drift-diffusion across the base given previously by Eq. (13). In the limit of weak compositional grading ($W_b \ll L_g$), the hole current density given by Eq. (15) goes to the expected limit $q(D_p/W_b)p(x_{ne})$, while for strong compositional grading ($W_b \gg L_g$), the hole current becomes $q(D_p/L_g)p(x_{ne})$.

The hole profile in the base given by Eq. (9) can now be rewritten by removing the explicit dependence on $p(x_{nc})$ using Eq. (14) to give

$$p(x)=p(x_{ne})\,\frac{S_{dp}L_g}{D_p}\left[1-\left(1-\frac{D_p}{v_sL_g}\right)e^{(x-x_{nc})/L_g}\right]. \tag{16}$$

Following Grinberg *et al.*,[16] but using the more comprehensive expression for the hole thermionic-emission-diffusion current following Stettler and Lundstrom,[15] we then set the drift-diffusion current in the base given by Eq. (15) equal to the thermionic-emission-diffusion current given by Eq. (10) to determine the hole concentration at the emitter end of the quasi-neutral base $p(x_{ne})$

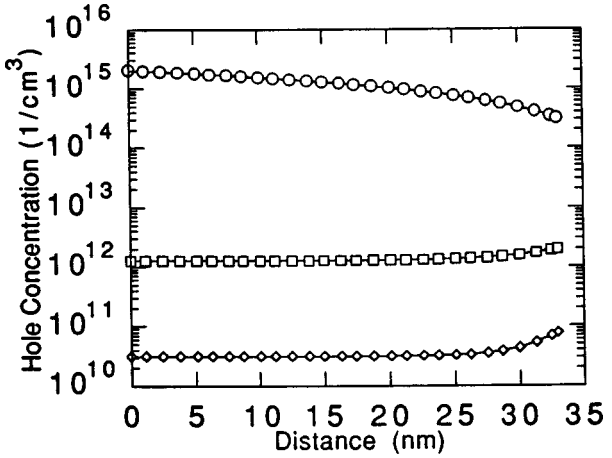

FIG. 4. Hole concentration profile across the quasi-neutral base for a fixed emitter-base bias of 0.8 V for compositional gradings of $W_b/L_g=0$ (○), 8 (□), and 12 (◇).

$$p(x_{ne})=\frac{p_0(x_{ne})S_P}{S_{dp}}\,e^{qV_{EB}/k_BT}, \tag{17}$$

where S_P is defined to be the combination of the hole effective velocities given by

$$\frac{1}{S_P}=\frac{1}{S_{ip}}+\frac{1}{S_{ep}}+\frac{1}{S_{dp}}+\frac{1}{v_s}. \tag{18}$$

Analogous to Eq. (10), the size of S_P is largely determined by the smallest of the effective velocities. As expected, Eq. (17) reduces to the familiar law of the junction when we consider the homojunction case with diffusion in the quasi-neutral base as the limiting process.

We can also get a final expression for the hole concentration at the collector end of the quasi-neutral base $p(x_{nc})$ by combining Eqs. (14) and (15) and then inserting Eq. (17) to give

$$p(x_{nc})=\frac{S_{dp}}{v_s}\,p(x_{ne})=\frac{p_0(x_{ne})S_P}{v_s}\,e^{qV_{EB}/k_BT}. \tag{19}$$

Since S_{dp} is typically less than v_s, $p(x_{nc})$ will be less than $p(x_{ne})$ as we expect for typical bipolar transistor operation. However, as seen in Fig. 3, when compositional grading is even moderately large ($W_b/L_g>2$), we can have S_{dp} larger than v_s so that from Eq. (19) we see that $p(x_{nc})$ can be greater than $p(x_{ne})$. This corresponds to a dynamic accumulation of holes at the collector end of the base brought about by the efficient transport of holes across the base aided by the quasi-field created by the compositional grading. Figure 3 also indicates that hole injection into the base is still limited by the combination of thermionic-field-emission (S_{ip}) and hole drift diffusion in the emitter space charge region (S_{ep}). As a result, for a significant range of base grading ($2<W_b/L_g<15$), the Pnp HBT operates with hole injection into the base limited by a combination of thermionic-field-emission and hole drift-diffusion in the emitter space charge region and a dynamic accumulation of holes at the collector end of the base limited by the transport of holes across the base-collector space charge region.

To illustrate these results, shown in Fig. 4 is the hole

profile across the base for several different base compositional gradings where we have assumed a constant emitter-base bias of 0.8 V. For weak compositional grading ($W_b/L_g \ll 1$), the hole profile is the normal decreasing hole concentration since the hole diffusion process is primarily responsible for carrier transport across the base. However, due to our requirement that the hole concentration at the collector end of the base be sufficient to carry the current, i.e., Eq. (14), the concentration gradient is not large and there is a significant hole concentration at the collector end of the base. For a moderate compositional grading ($W_b/L_g=8$), the hole profile is nearly flat since the quasi-field arising from the compositional grading is effective in sweeping the carriers across the base. As can be seen, the quasi-field also causes the hole concentration at the emitter end of the base $p(x_{ne})$ to be smaller. For stronger compositional grading ($W_b/L_g>13$), the hole profile is nearly flat across most of the base, but shows an accumulation at the collector end of the base. As described above, this is due to the efficient transport of holes across the base as a result of diffusion and drift in the quasi-electric field. The extent of this dynamic accumulation of holes at the collector end of the base will also be a function of the base width as seen from Eq. (19) where $p(x_{nc})$ is seen to be proportional to S_{dp} which is given by Eq. (13). That is, for a fixed energy gap grading across the base, an increase in the base width will reduce D_p/L_g and correspondingly reduce S_{dp} which will decrease $p(x_{nc})$ and the dynamic accumulation of holes at the collector end of the base.

III. TERMINAL CURRENTS AND CURRENT GAIN

Using the above described results, we can proceed to determine the device's terminal currents. For the emitter current, the electron current density due to back injection into the emitter must be added to the hole component given by Eq. (10). Similar to the above analysis for holes, the emitter thermionic emission electron current density following Grinberg *et al.*[16,17] is given by

$$J_{ne}=-qv_e N_{CB}\left(\frac{n(x_j^-)}{N_{CE}}-\frac{n(x_j^+)}{N_{CB}}\,e^{-\Delta E_C/k_BT}\right), \tag{20}$$

where $n(x_j^-)$ and $n(x_j^+)$ are the electron concentrations on the emitter and base sides, respectively, of the emitter-base junction immediately adjacent to the heterojunction at x_j, N_{CE} and N_{CB} are the conduction band density of states for the emitter and base regions, respectively, and ΔE_C is the conduction band discontinuity. The mean thermal electron velocity v_e in Eq. (20) is given by $v_e \equiv \sqrt{(k_BT)/(2\pi m_e^*)}$, where m_e^* is the electron density of states effective mass in the base. Since the electron effective mass is almost a factor of two larger in the emitter than in the base for the InP-based material system, N_{CE} and N_{CB} are not equal and we cannot neglect this difference as we did previously for the holes. Then, relating the electron concentrations on either side of the heterojunction to their respective values at the edges of the emitter-base space charge region using the Boltzmann relation, we get

$$n(x_j^-)=n(x_{pe})e^{qV_{jp}/k_BT} \quad \text{and} \quad n(x_j^+)=n(x_{ne})e^{-qV_{jn}/k_BT}. \tag{21}$$

We can then rewrite Eq. (20) as

$$J_{ne}=qS_{\text{in}}[n_0(x_{pe})(e^{qV_{\text{EB}}/k_BT}-1)-\Delta n(x_{pe})], \tag{22}$$

where $\Delta n(x_{pe})$ is the excess and $n_0(x_{pe})$ is the thermal equilibrium electron concentration at the end of the space charge region in the emitter and S_{in} is the electron heterojunction interface velocity defined as

$$\begin{aligned} S_{\text{in}} &= v_e\,\frac{N_{CB}}{N_{CE}}\,e^{qV_{jp}/k_BT} \\ &\approx v_e\,\frac{N_{CB}}{N_{CE}}\left(\frac{N_E N_B}{n_{ie}^2}\right)e^{-\Delta E_C/k_BT}e^{-qV_{\text{EB}}/k_BT}, \end{aligned} \tag{23}$$

where N_E and N_B are the emitter and base doping, respectively, n_{ie} is the intrinsic carrier concentration in the emitter and V_{EB} is the applied emitter-base junction bias. The latter approximation in Eq. (23) arises because the band bending on the emitter side V_{jp} can be approximated by $V_{bi}-V_{\text{EB}}$, where $N_B \gg N_E$, where V_{bi} is the base-emitter junction built-in potential

$$\begin{aligned} V_{\text{bi}} &= \frac{\Delta E_V-\Delta E_C}{2q}+\frac{k_BT}{q}\ln\left(\frac{N_E N_B}{n_{ie}n_{ib}}\right) \\ &= \frac{-\Delta E_C}{q}+\frac{k_BT}{q}\ln\left(\frac{N_E N_B}{n_{ie}^2}\right). \end{aligned} \tag{24}$$

The electron minority carrier profile in the emitter is given by the usual diffusion profile so that on matching the thermionic emission and diffusion currents, the electron component of the emitter current density is given by[19]

$$J_{ne}=\frac{qS_{\text{dne}}n_0(x_{pe})}{1+(S_{\text{dne}}/S_{\text{in}})\coth(W_e/L_{ne})}\,(e^{qV_{\text{EB}}/k_BT}-1), \tag{25}$$

where we have taken into account the finite width of the emitter W_e. In Eq. (25) S_{dne} is the electron diffusion velocity in the emitter given by D_{ne}/L_{ne}, where D_{ne} and L_{ne} are the electron diffusion constant and length in the emitter, respectively, and $n_0(x_{pe})$ is the thermal equilibrium electron concentration in the bulk emitter. The total emitter current density is then given by

$$\begin{aligned} J_e &= J_p+J_{ne} \\ &= qp_0(x_{ne})S_P e^{qV_{\text{EB}}/k_BT} \\ &\quad +\frac{qS_{\text{dne}}n_0(x_{pe})}{1+(S_{\text{dne}}/S_{\text{in}})\coth(W_e/L_{ne})}\,(e^{qV_{\text{EB}}/k_BT}-1). \end{aligned} \tag{26}$$

For the collector current, since we have a simple p-n homojunction, the electron current density for the device in the normal, forward active mode is given by

$$J_{nc}=\frac{qD_{nc}}{L_{nc}}\,n_0(x_{nc})\coth\left(\frac{W_c}{L_{nc}}\right), \tag{27}$$

where D_{nc} and L_{nc} are the electron diffusion constant and length in the collector, respectively, $n_0(x_{nc})$ is the thermal

equilibrium electron concentration in the bulk collector and W_c is the width of the neutral collector region. The total collector current is then the sum of the hole current density given in Eq. (10) and the electron component given in Eq. (27) so

$$J_c = J_p + J_{nc} = qS_P p_0(x_{ne}) e^{qV_{EB}/k_B T} + \frac{qD_{nc}}{L_{nc}} n_0(x_{nc}) \coth\left(\frac{W_c}{L_{nc}}\right). \quad (28)$$

Neglecting the recombination currents, the base current is given by the difference of the total emitter and collector currents so that on substituting Eqs. (26) and (28) we obtain

$$J_b = J_{ne} - J_{nc} = \frac{qS_{\text{dne}} n_0(x_{pe})}{1 + (S_{\text{dne}}/S_{\text{in}}) \coth(W_e/L_{ne})} \times (e^{qV_{EB}/k_B T} - 1) - \frac{qD_{nc}}{L_{nc}} n_0(x_{nc}) \coth\left(\frac{W_c}{L_{nc}}\right). \quad (29)$$

From the terminal current expressions for the collector and the base currents given in Eqs. (27) and (28) we can obtain an expression for the small signal current gain

$$\beta = \frac{p_0(x_{ne})}{n_0(x_{pe})} \frac{S_P}{S_{\text{dne}}} \left[1 + \frac{S_{\text{dne}}}{S_{\text{in}}} \coth\left(\frac{W_e}{L_{ne}}\right)\right]. \quad (30)$$

In the limit of a homojunction for the emitter-base junction, no compositional grading in the base and no finite emitter width effect, $S_p \rightarrow S_{dp} = D_p/W_b$ and β reduces to the usual result.

What is neglected in the expressions for the terminal current densities given in Eqs. (26), (28), and (29) are the contributions, particularly to the base current, of the recombination current components. Inclusion of the recombination currents gives[18,19,25]

$$\begin{aligned} J_e &= J_p + J_{ne} + J_{scr} + J_{sr} + J_{ire} + J_{irb} + J_{br} + J_{rr}, \\ J_c &= J_p + J_{nc}, \\ J_b &= J_{ne} - J_{nc} + J_{scr} + J_{sr} + J_{ire} + J_{irb} + J_{br} + J_{rr}, \end{aligned} \quad (31)$$

where J_{rr} and J_{br} are the radiative and nonradiative recombination current densities in the quasi-neutral base, respectively, J_{sr} is the recombination current density at the surface, J_{scr} is the recombination current density in the emitter-base space charge region, and J_{irb} and J_{ire} are the interface recombination current densities on the base and emitter side, respectively, of the emitter-base heterojunction. While Auger recombination is not explicitly included in Eq. (31), the effects of the base doping on the hole minority carrier lifetime in the base are included based on a fit to experimental data so that the effects of Auger recombination are incorporated in the nonradiative base recombination current J_{br}. Since compositional grading in the base modifies the minority carrier hole profile in the base, the base recombination components are reexamined here.

The nonradiative base recombination current can be described starting from[19,25]

$$J_{br} = q \int_{x_{ne}}^{x_{nc}} \frac{[p(x) - p_0(x)]}{\tau_p} dx, \quad (32)$$

where τ_p is the minority carrier hole lifetime in the base and $p_0(x)$ is the thermal equilibrium minority carrier concentration at x, which varies due to the compositional grading in the base and is given by

$$p_0(x) = \frac{n_i^2(x)}{N_B} = \frac{N_{\text{CB}} N_{\text{VB}}}{N_B} e^{-E_g(x)/k_B T}. \quad (33)$$

Here N_{CB} and N_{VB} are the conduction and valence band densities of states, respectively, in the base which are taken to be constant by neglecting the variation in the carrier effective masses across the base. Since the base composition is linearly graded, $E_g(x)$ can be written as

$$E_g(x) = E_g(x_{nc}) - k_B T \frac{(x - x_{nc})}{L_g} \quad (34)$$

and on substituting Eqs. (33) and (34) in (32) and integrating using Eq. (16) for $p(x)$ we get

$$J_{br} = \frac{qL_g W_b S_P}{D_p \tau_p} \left[1 - \frac{L_g}{W_b}\left(1 - \frac{D_p}{v_s L_g}\right)(1 - e^{-W_b/L_g})\right] \times p_0(x_{ne}) e^{qV_{EB}/k_B T} - \frac{q n_{i0}^2 L_g}{\tau_p N_B} (1 - e^{-W_b/L_g}), \quad (35)$$

where n_{i0} is the intrinsic carrier concentration at the collector end of the base given by

$$n_{i0}^2 = N_{\text{CB}} N_{\text{VB}} e^{-E_g(x_{nc})/k_B T}. \quad (36)$$

Similarly, there is also a radiative recombination component to the base current. Following our above analysis for the nonradiative component we get[25]

$$J_{rr} = qBN_B \int_{x_{ne}}^{x_{nc}} \left[p(x) - \frac{n_i^2(x)}{N_B}\right] dx, \quad (37)$$

where B is the radiative recombination coefficient. Substituting from Eqs. (33) and (34) and integrating using Eq. (16) for $p(x)$ we get

$$J_{rr} = \frac{qBN_B L_g W_b S_P}{D_P} \left[1 - \frac{L_g}{W_b}\left(1 - \frac{D_p}{v_s L_g}\right)(1 - e^{-W_b/L_g})\right] \times p_0(x_{ne}) e^{qV_{EB}/k_B T} - q n_{i0}^2 L_g B (1 - e^{-W_b/L_g}). \quad (38)$$

The emitter-base space charge region recombination current J_{scr} can also be found starting from[19,25]

$$J_{scr} = \tfrac{1}{2} qN_{\text{tr}} \sigma v_e W_0 \sqrt{n(x_{ne}) p(x_{ne})}, \quad (39)$$

where σ is the carrier capture cross section, N_{tr} is the recombination trap density, v_e is the electron thermal velocity defined earlier, and W_0 is the fraction of the width of the emitter-base space charge region W_{scr} in which recombination perdominately occurs and is given by

$$W_0 = W_{scr}\left[\frac{\pi k_B T}{q(V_{\text{bi}} - V_{\text{EB}})}\right], \quad (40)$$

where V_{bi} and V_{EB} are the emitter-base junction built-in potential and applied bias, respectively. Since the base is more strongly doped than the emitter, the penetration of the space charge region into the base is negligibly small so that the

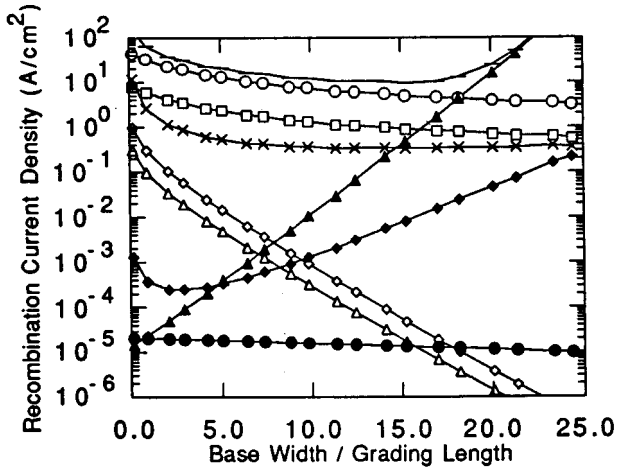

FIG. 5. Base recombination currents [nonradiative J_{br} (○) and radiative J_{rr} (□), space charge region J_{scr} (◇), surface J_{sr} (△), emitter side interface J_{ire} (♦), base side interface J_{irb} (x)], electron back injection J_{ne} (▲), electron collector leakage J_{nc} (●) and total base current (no symbol) as a function of compositional base grading (W_b/L_g).

TABLE I. Material parameters for Pnp InAlAs/InGaAs heterojunction bipolar transistor.

Emitter	Base	Collector
InAlAs p-type	InGaAs n-type	InGaAs p-type
$E_g=1.47$ eV	$E_g(x_{nc})=0.75$ eV	$E_g=0.75$ eV
$\chi_E=4.1$ eV	$\chi_B(x_{nc})=4.58$ eV	$\chi_C=4.58$ eV
$N_E=1\times10^{18}/\text{cm}^3$	$N_B=5\times10^{18}/\text{cm}^3$	$N_C=5\times10^{16}/\text{cm}^3$
$W_e=0.14$ μm	$W_b=0.06$ μm	$W_c=0.3$ μm
$L_{ne}=3.8$ μm	$L_p=0.48$ μm	$L_{nc}=5.2$ μm
$D_{ne}=14.5$ cm^2/s	$D_p=2.6$ cm^2/s	$D_{nc}=300$ cm^2/s
$\mu_h=59$ cm^2/V s	$\mu_p=100$ cm^2/V s	$\mu_n=1160$ cm^2/V s
	$m_e^*=0.041m_0$	$m_e^*=0.041m_0$
$m_{pe}^*=0.48m_0$	$m_h^*=0.47m_0$	$m_h^*=0.47m_0$
$n_{ie}=9.3\times10^5/\text{cm}^3$	$n_{i0}=6.5\times10^{11}/\text{cm}^3$	
$s_e=10$ cm/s	$s_b=10$ cm/s	
	$\tau_p=0.9$ ns	$v_s=4.5\times10^6$ cm/s
$\rho_{ec}=1\times10^{-6}$ Ω cm^2	$\rho_{bc}=1\times10^{-7}$ Ω cm^2	$\rho_{cc}=1\times10^{-6}$ Ω cm^2
$N_{tr}=4\times10^{16}/\text{cm}^2$	$B=4.2\times10^{-11}$ cm^3 s	
$\sigma=4\times10^{-17}$ cm^2	$s_0L_s=2\times10^{-4}$ cm^2/s	

effects of compositional grading have been neglected in obtaining Eq. (39) and the following recombination currents. Substituting from Eqs. (33) and (17) for the carrier concentrations and simplifying we get

$$J_{scr}=\frac{1}{2}\,qN_{\text{tr}}\sigma v_e W_0 n_{i0} e^{-W_b/2L_g}\sqrt{\frac{S_P}{S_{dp}}}\,e^{qV_{BE}/2k_BT}. \quad (41)$$

Similarly, the surface recombination current can be written as[19,25]

$$J_{sr}=qs_0L_s\,\frac{P_E}{A_E}\,n_{i0}e^{-W_b/2L_g}\sqrt{\frac{S_P}{S_{dp}}}\,e^{qV_{BE}/2k_BT}, \quad (42)$$

where $P_E(A_E)$ is the emitter mesa perimeter (area), s_0 is the surface recombination velocity, and L_s is the surface diffusion length. Finally, there are additional base current components associated with recombination at the emitter-base heterojunction interface, i.e., J_{ire} and J_{irb} associated with recombination at the interface on the emitter and base sides, respectively, that are given by[19,25]

$$J_{ire}=qs_ep_0(x_{pe})e^{-qV_{\text{bip}}/k_BT}\left[\frac{S_P}{S_{dp}}\,e^{qV_{BE}/k_BT}-1\right],$$

$$J_{irb}=qs_bp_0(x_{ne})e^{qV_{\text{bin}}/k_BT}\left[\frac{S_P}{S_{dp}}\,e^{qV_{BE}/k_BT}-1\right], \quad (43)$$

where s_e and s_b are the interface recombination velocities on the emitter and base sides heterojunction, respectively, and V_{bin} and V_{bip} are the fractions of the emitter-base built-in potential on the emitter and base sides, respectively.

Utilizing the above results, we can examine the various contributions to the base current. These are displayed in Fig. 5 as a function of compositional grading at a constant collector current density of 10^4 A/cm^2. The material parameters used in the calculations are summarized in Table I and the device structure is similar to that of Stanchina *et al.*[8,9] The results show that in the absence of compositional base grading, the base current is dominated by nonradiative recombination in the quasi-neutral base region as frequently seen for InP-based Npn HBTs. As the extent of compositional grading in the base increases, the nonradiative recombination current as well as most of the other components decrease in size. This effect results from the fact that with increased compositional grading, the quasi-electric field is enhanced and more effectively sweeps holes out of the quasi-neutral base reducing the hole concentration across the entire width of the base as seen in Fig. 4. This effect reduces not only the nonradiative and radiative components as expected Eqs. (35) and (38), but also the interface and space charge region recombination components. The latter results from the increasing quasi-field which reduces the hole concentration at the emitter end of the base $p(x_{ne})$ as seen in Fig. 4, which reduces the interface recombination current as seen from Eq. (39). Similarly, the increasing base quasi-field increases the effective hole diffusion velocity in the base S_{dp} as seen in Fig. 3, which causes the interface recombination current to decrease as seen from Eq. (43). Finally, the quasi-field in the base also drives holes away from the exposed base surface between the emitter mesa and the base metal contact and so reduces the base surface recombination current as seen in Fig. 4 and Eq. (42).

By contrast, the base current component due to electron back injection into the emitter J_{ne} given by Eq. (25) rises steadily as the extent of base grading increases. The interface recombination on the emitter side of the heterojunction interface also increases, but remains small. Since the emitter energy band gap is fixed, with increased base grading the conduction band discontinuity is reduced so that S_{in} given by Eq. (23) is enlarged and J_{ne} given by Eq. (25) increases. As a result, at large enough base grading ($W_b/L_g>18$), electron back injection into the emitter dominates the base current and the base current begins to increase. The net effect of increasing base grading is that the total base current goes through a broad minimum. The corresponding effects of compositional grading on the dc current gain for the transistor are seen in Fig. 6. As expected, the current gain goes

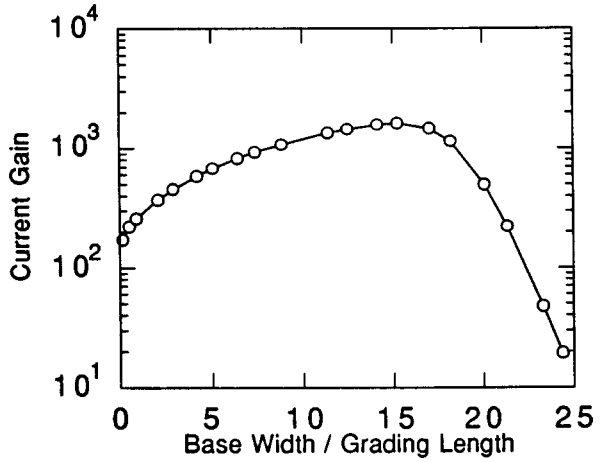

FIG. 6. DC current gain (○) as a function of base grading (W_b/L_g) including base recombination current components for a collector current density of 10^4 A/cm^2.

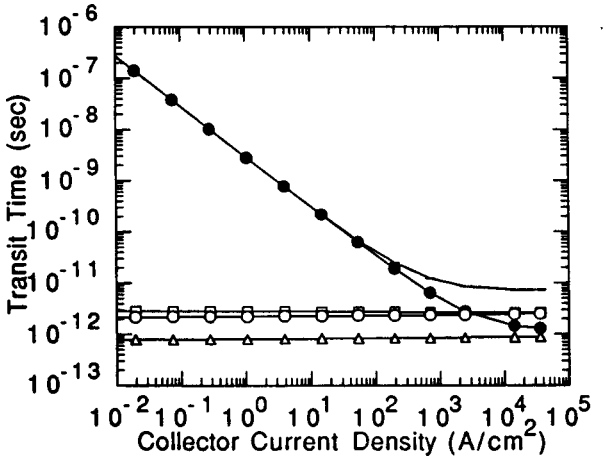

FIG. 7. Transit time components [base transit time τ_b (○), emitter charging time τ_e (●), collector delay time τ_{bc} (□) and collector charging time τ_c (△)] and total emitter-to-collector delay time τ_{ec} (no symbol) versus collector current density in the case of no compositional grading in the base.

through a broad maximum as the base grading is enlarged. The enhancing effect of the base grading is significant producing nearly an order of magnitude increase in the current gain reaching a maximum of 1700 near $W_b/L_g=15$.

IV. BASE TRANSIT TIME AND CUTOFF FREQUENCY

The incorporation of grading in the base also impacts the base transit time and so the high frequency performance capabilities of the device. For *Pnp* HBTs, the low hole diffusion constant in the base makes the hole base transit time a dominant component in the emitter-to-collector delay time. Following Pulfrey[20,26] and Ferry *et al.*,[27] we can calculate the base transit time from

$$\tau_b=\int_{x_{ne}}^{x_{nc}}\frac{1}{v_h(x)}\,dx, \tag{44}$$

where $v_h(x)$ is the average hole velocity at x in the base which is related to the hole current density J_p by

$$J_p=qv_h(x)[p(x)-p_0(x)], \tag{45}$$

where the quantity in brackets is the excess hole concentration at x. Due to compositional grading in the base, the thermal equilibrium concentration p_0 is also a function of x and combining Eqs. (33) and (34) we can write

$$p_0(x)=\frac{n_{i0}^2}{N_B}\,e^{(x-x_{nc})/L_g}, \tag{46}$$

where n_{i0} is the intrinsic carrier concentration at the collector end of the quasi-neutral base. Solving Eq. (45) for $v_h(x)$ and substituting into Eq. (44), we can integrate Eq. (44) using Eq. (16) for $p(x)$ and Eq. (46) for $p_0(x)$ to obtain

$$\tau_b=\frac{W_b^2}{2D_p}\left\{\frac{2L_g}{W_b}\left[1-\frac{L_g}{W_b}\left(1-\frac{D_p}{v_sL_g}\right)(1-e^{-W_b/L_g})\right]\right\}$$
$$-\frac{n_{i0}^2L_ge^{-qV_{EB}/k_BT}}{S_PN_Bp_0(x_{ne})}(1-e^{-W_b/L_g}), \tag{47}$$

where we have used Eqs. (15) and (17) to simplify the result. The last term in Eq. (47) arises from the variation in the intrinsic concentration across the base region. In the limit of no compositional grading in the base, this reduces to the usual result $W_b^2/2D_p+W_b/V_s$.[24] However, when compositional grading is used, the quasi-field in the base aids the hole transport across the base and can significantly reduce the base transit time as shown below.

Not included in the present model are the effects on the base transit time of hot hole injection across the valence band discontinuity and ballistic transport across the base. The present model includes only drift diffusion across the base of thermalized holes. For *Npn* HBTs, the effects of hot electron injection and ballistic transport have been shown to impact the base transit time for InP-based devices.[28] Due to the small base widths, e.g., 35 nm, and the large valence band discontinuities (0.24 and 0.34 eV for InAlAs/InGaAs and InP/InGaAs, respectively), similar effects may also be important for the *Pnp* HBTs. There have also been some previous reports of ballistic hole transport.[29–31] Further study is needed to examine the extent of these effects and to incorporate the effects in the analysis of the base transit time.

The cutoff frequency for the HBT is determined by the total emitter-to-collector delay time τ_{ec} given by[32]

$$\tau_{ec}=\frac{k_BT}{qI_C}\{C_{be}+C_{bc}\}+\tau_b+\tau_{bc}+\{R_e+R_c\}C_{bc}, \tag{48}$$

where C_{be} and C_{bc} are the emitter and collector junction depletion capacitances, respectively, R_e and R_c are the emitter and collector series resistances, I_c is the dc collector current and τ_{bc} is the base-collector delay time given by $W_{bc}/2v_s$. The emitter and collector resistances were modeled following Ho and Pulfrey[20] using the parameters given in Table I, where ρ_{ec}, ρ_{bc}, and ρ_{cc} are the emitter, base, and collector contact resistivities. Seen in Fig. 7 is a plot of the transit time components and the τ_{ec} as a function of the collector current density for the device of Stanchina *et al.*[8] for the case of no compositional grading in the base. As can be seen, the base transit time is one of two dominant components so that use of compositional grading can be effective in reducing the total τ_{ec} and improving the cutoff frequency

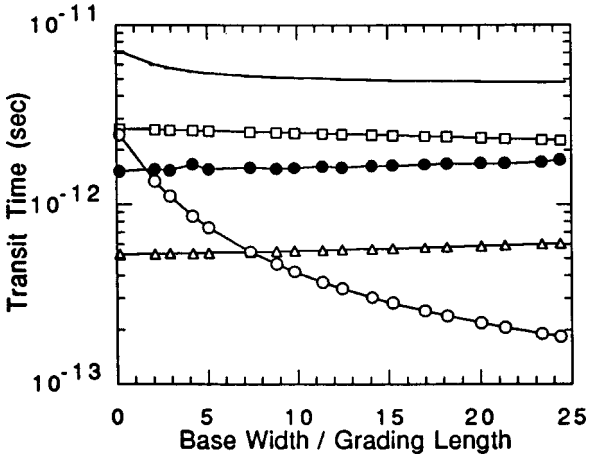

FIG. 8. Transit time components [base transit time τ_b (○), emitter charging time τ_e (●), collector delay time τ_{bc} (□) and collector charging time τ_c (△)] and total emitter-to-collector delay time τ_{ec} (no symbol) as a function of the compositional grading in the base for a collector current density of 10^4 A/cm^2.

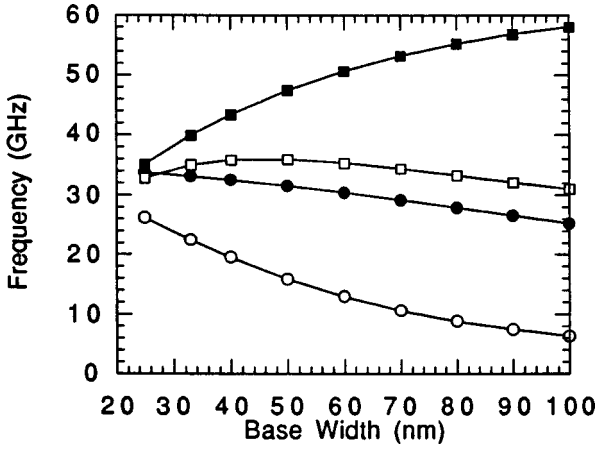

FIG. 10. Cutoff frequency without (○) and with base grading (●) and maximum frequency of oscillation without (□) and with base grading (■) as a function of base width for a fixed base doping of 7×10^{18}/cm^3 for a base grading of $W_b/L_g=24$ for a collector current density of 10^4 A/cm^2.

of the device. As an illustration, seen in Fig. 8 is a plot of the base transit time using Eq. (47) as a function of the base grading at a fixed collector current density of 10^4 A/cm^2. For comparison, also shown are the other transit time components, which are independent of the base grading, and the total emitter-to-collector transit time. The effects of base grading on τ_b are dramatic producing a reduction of more than an order of magnitude. However, beyond a grading of $W_b/L_g=8$, there is little benefit on device speed of increased grading as the collector delay time dominates the τ_{ec}.

Figure 9 is a plot of the cutoff frequency versus the collector current density for a series of three compositional gradings in the base region ($W_b/L_g=0$, 8, and 24). Clearly, the cutoff frequency is significantly enhanced (by more than 50%) when the compositional grading is employed ($W_b/L_g=8$). However, there is only a modest additional improvement when the grading is increased from $W_b/L_g=8$ to 24, as expected from Fig. 8.

Seen in Fig. 10 are the cutoff frequency f_T and maximum frequency of oscillation $f_{\max}$ for a collector current density of 10^4 A/cm^2 as a function of base width for a fixed base doping of 7×10^{18}/cm^3 for no compositional grading and a grading of $W_b/L_g=24$. The $f_{\max}$ was calculated from the f_T using

$$f_{\max}=\sqrt{\frac{f_T}{8\pi(R_BC_C)_{\text{eff}}}}, \tag{49}$$

where $(R_BC_C)_{\text{eff}}$ is the effective base resistance-collector capacitance product defined by Ho and Pulfrey.[20] For both the f_T and $f_{\max}$ frequencies, the effects of base grading are significant, particularly for larger base widths. At a base width of 50 nm, the cutoff frequency is more than doubled while the maximum frequency of oscillation increases by approximately 30%. Similarly, seen in Fig. 11 are the effects of compositional grading ($W_b/L_g=24$) versus no grading on the two frequencies as the base doping is varied for a fixed base width of 33 nm. Again, the effects of compositional base grading are significant, particularly at the highest dop-

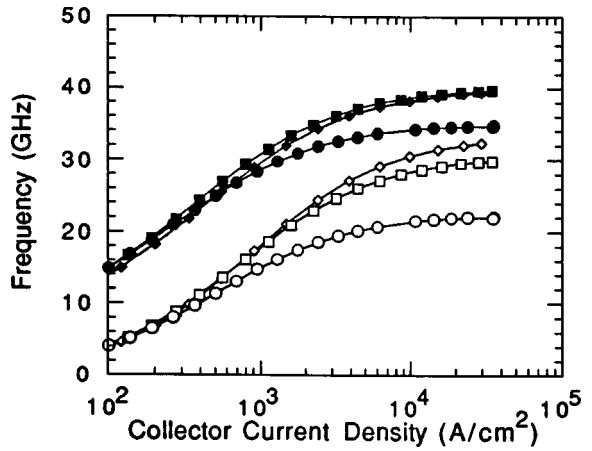

FIG. 9. Cutoff frequency for $W_b/L_g=0$ (○), 8 (□), and 24 (◇) and maximum frequency of oscillation for $W_b/L_g=0$ (●), 8 (■), and 24 (◆) vs collector current density.

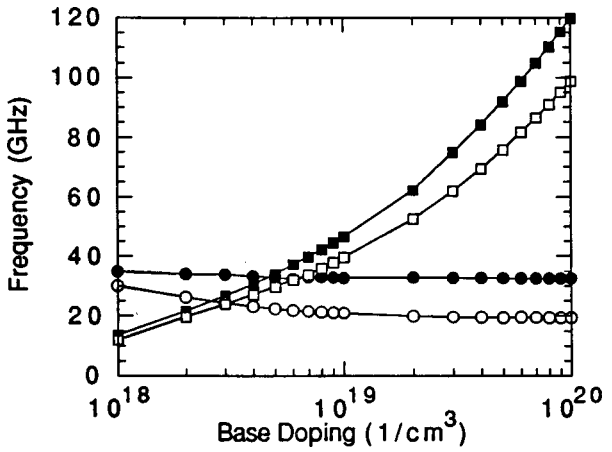

FIG. 11. Cutoff frequency without (○) and with base grading (●) and maximum frequency of oscillation without (□) and with base grading (■) as a function of base doping for a fixed base width of 33 nm for a base grading of $W_b/L_g=24$ for a collector current density of 10^4 A/cm^2.

ing levels. At a base doping of $2\times10^{19}/\mathrm{cm}^3$, the cutoff frequency is enhanced by approximately 50%, while the maximum frequency of oscillation increases by approximately 10%.

V. CONCLUSION

In summary, we have presented an analytical model for the *Pnp* HBT that takes into account thermionic-emission-diffusion of holes across the emitter-base heterojunction and matches this hole injection with the drift-diffusion current in the base to determine self-consistently the hole current density. The effects of compositional grading of the base were also incorporated in the determination of the base recombination currents. The results were used to examine the effects of base grading on the transistor's current–voltage characteristics and current gain. An optimum base grading was found where the reduction in the base recombination currents is significant, but the effects of enhanced electron back injection into the emitter not yet dominant. Also, the effects of base grading on the device's high frequency performance were analyzed and shown to be effective in reducing base transit time and improving the cutoff frequency and maximum frequency of oscillation.

The feasibility of the use of compositional grading in the base for *Npn* InP-based HBTs has recently been demonstrated by Kurishima *et al.*[28] and Ohkubo *et al.*[33] using strained $In_{1-x}Ga_xAs$. Chirped superlattices have also been successfully employed to compositionally grade the emitter-base and base-collector junction in *Npn* HBTs.[34,35] Further study is needed of hot hole injection and ballistic transport effects to determine the optimum base grading for the *Pnp* HBT.

As a final note, the model of tunneling and thermionic emission presented in this article assumes an effective mass for carriers equal to the density of states effective mass for holes. A more thorough investigation should include an independent calculation of the light and heavy hole tunneling across the emitter-base junction. We have used a scattering matrix approach to this problem[36] and have shown that for $InP/In_{0.53}Ga_{0.47}$ As heterojunctions, the split-off spin-orbit band can have a dramatic influence on the tunneling of heavy and light holes and on the energy distribution of the carriers injected into the base.[37] This in turn will influence the base transit time and hence the high frequency response of the device. Our results will be presented in a forthcoming publication.

ACKNOWLEDGMENT

This work was supported by the National Science Foundation under Grant No. ECS-9525942.

[1] J. Bales, IEEE J. Solid-State Circuits **32**, 1470 (1997).
[2] D. B. Slater, P. M. Enquist, F. E. Najjar, M. Y. Chen, and J. A. Hutchby, IEEE Electron Device Lett. **11**, 146 (1990).
[3] H. Q. Tserng, D. G. Hill, and T. S. Kim, IEEE Microwave Guid. Wave Lett. **3**, 45 (1993).
[4] D. G. Hill, T. S. Kim, and H. Q. Tserng, IEEE Electron Device Lett. **14**, 185 (1993).
[5] G. J. Sullivan, M. F. Chang, N. H. Sheng, R. J. Anderson, N. L. Wang, K. C. Wang, J. A. Higgins, and P. M. Asbeck, IEEE Electron Device Lett. **11**, 463 (1990).
[6] W. Liu and C. Dai, Jpn. J. Appl. Phys., Part 2 **31**, L452 (1992).
[7] G. B. Gao, D. J. Roulston, and H. Morkoc, Solid-State Electron. **33**, 1209 (1990).
[8] W. E. Stanchina, R. A. Metzger, M. W. Pierce, J. F. Jensen, L. G. McCray, R. Wong-Quen, and F. Williams, Proceedings of the Fifth International Conference on InP and Related Materials, 1993, p. 569.
[9] W. E. Stanchina, R. A. Metzger, D. B. Rensch, L. M. Burns, J. F. Jensen, R. H. Walden, L. E. Larson, and P. T. Greiling, GOMAC-91 Digest of Papers, 1991, p. 385.
[10] L. M. Lunardi, S. Chandrasekhar, and R. A. Hamm, IEEE Electron Device Lett. **14**, 19 (1993).
[11] S. Shi, K. P. Roenker, T. Kumar, M. M. Cahay, and W. E. Stanchina, IEEE Trans. Electron Devices **43**, 1466 (1996).
[12] S. Datta, S. Shi, K. P. Roenker, M. M. Cahay, and W. E. Stanchina, Proceedings of the Ninth International Conference on Indium Phosphide and Related Materials, 1997, p. 392.
[13] D. B. Slater, P. M. Enquist, J. A. Hutchby, A. S. Morris, and R. J. Trew, IEEE Electron Device Lett. **15**, 91 (1994).
[14] W. Liu, D. Hill, D. Costa, and J. S. Harris, IEEE Microwave Guid. Wave Lett. **2**, 331 (1992).
[15] M. A. Stettler and M. S. Lundstrom, IEEE Trans. Electron Devices **41**, 592 (1994).
[16] A. A. Grinberg, M. S. Shur, R. J. Fischer, and H. Morkoc, IEEE Trans. Electron Devices **31**, 1758 (1984).
[17] A. A. Grinberg and S. Luryi, IEEE Trans. Electron Devices **40**, 859 (1993).
[18] B. R. Ryum and I. M. Abdel-Motaleb, Solid-State Electron. **34**, 1125 (1991).
[19] B. R. Ryum and I. M. Abdel-Motaleb, Solid-State Electron. **33**, 869 (1990).
[20] S. C. M. Ho and D. L. Pulfrey, IEEE Trans. Electron Devices **36**, 2173 (1989).
[21] J. A. Hutchby, IEEE Electron Device Lett. **7**, 108 (1986).
[22] D. A. Sunderland and P. D. Dapkus, IEEE Trans. Electron Devices **34**, 367 (1987).
[23] J. S. Yuan, Solid-State Electron. **34**, 1347 (1991).
[24] M. B. Das, in *HEMTs and HBTs: Devices, Fabrication and Circuits*, edited by F. Ali and A. Gupta (Artech House, Boston, 1991), Chap. 4, p. 191.
[25] B. R. Ryum and I. M. Abdel-Motaleb, IEE Proc.-G: Circuits, Devices Syst. **138**, 115 (1991).
[26] O. S. Ang and D. L. Pulfrey, Solid-State Electron. **34**, 1325 (1991).
[27] D. K. Ferry, L. A. Akers, and E. W. Greeneich, in *Ultra Large Scale Integrated Microelectronics* (Prentice–Hall, Englewood Cliffs, NJ, 1988), p. 112.
[28] K. Kurishima, H. Nakajima, S. Yamahata, T. Kobayashi, and Y. Matsuoka, Jpn. J. Appl. Phys., Part 1 **34**, 1221 (1995).
[29] S. L. Chuang, Phys. Rev. **40**, 10379 (1989).
[30] C. Y. P. Chao and S. L. Chuang, Phys. Rev. B **43**, 7027 (1991).
[31] K. Brennan and K. Hess, Phys. Rev. B **29**, 5581 (1984).
[32] W. Liu, D. Costa, and J. S. Harris, Solid-State Electron. **35**, 541 (1992).
[33] M. Ohkubo, J. Osabe, N. Ikeda, and T. Ninomiya, Proceedings of the Ninth International Conference on Indium Phosphide and Related Materials, 1997, p. 641.
[34] H. Hafizi, W. E. Stanchina, R. A. Mtezger, P. A. MacDonald, and F. Williams, Jr., IEEE Trans. Electron Devices **40**, 1583 (1993).
[35] K. Yang, G. O. Munns, X. Wang, and G. I. Haddad, Proceedings of the Ninth International Conference on Indium Phosphide and Related Materials, 1997, p. 645.
[36] T. Kumar, M. M. Cahay, and K. P. Roenker, Phys. Rev. B **56**, 4836 (1997).
[37] S. Ekbote, M. M. Cahay, and K. P. Roenker, Phys. Rev. B (submitted).